

Optimal Segmentation of the Optic Nerve Head from Stereo Retinal Images

Michael B. Merickel Jr.^a, Xiaodong Wu^{a,b}, Milan Sonka^{a,c}, Michael Abramoff^c

^aThe University of Iowa, Dept. of Electrical and Computer Eng., Iowa City, IA, USA

^bThe University of Iowa, Dept. of Radiation Oncology, Iowa City, IA, USA

^cThe University of Iowa, Dept. of Ophthalmology and Visual Sciences, Iowa City, IA, USA

ABSTRACT

Early detection of glaucoma is essential to minimizing the risk of visual loss. It has been shown that a good predictor of glaucoma is the cup-to-disc ratio of the optic nerve head. This paper presents a highly automated method to segment the ‘rim’ (disc) and ‘cup’ from the optic nerve head in stereo images and calculate the cup-to-disc ratio. In this approach, the optic nerve head is *unwrapped* in polar coordinates and represented as a graph. Utilizing a novel and efficient graph searching technique for determining globally optimal closed-paths and an intelligent cost function, the rim and the cup are segmented from the stereo images. The results offer a more intuitive quantitative analysis compared to current planimetry-based techniques because the ophthalmologist can view the segmented images along with the derived cup-to-disc ratio.

Keywords: image segmentation, optic nerve head, graph searching, optimal border detection

1. INTRODUCTION

Glaucoma affects approximately 2-3% of the US population and is the second leading cause of blindness in the US. The risk of visual field loss due to glaucoma is minimized by early diagnosis and optimal treatment methods [1]. The optic nerve head is a three-dimensional structure characterized by a peripheral ‘rim’ (disc) and a central depression called the ‘cup’. Certain characteristics of the optic nerve head facilitate early detection of glaucoma.

Currently, the gold standard for diagnosis and treatment follow-up of glaucoma is optic nerve planimetry [1]. The method determines the extent of the rim and cup through manual evaluation of stereo 2-D retinal images of the optic nerve head by an ophthalmologist. The technique is time-consuming and tedious and introduces large variability due to the need for human interpretation [2]. It is clear that an automated, quantitative method is necessary for analyzing the optic nerve head in stereo photographs.

We attempt to develop an algorithm that is capable of providing intuitive results using stereo data. In this paper we model the optic nerve head segmentation as a search for optimal closed paths in a weighted directed graph and develop a new and efficient algorithm for detecting the rim and cup in stereo photographs of the optic nerve head. We have also developed a method to incorporate a priori pixel classification information of the nerve head into the cost function which greatly improves the accuracy of the segmentation. The underlying Chen, Wang, Wu [3] graph algorithm had never been implemented as a computer program or applied to medial image segmentation problems before.

The algorithm was validated in 101 datasets from patients with a diagnosis of glaucoma. The theoretical advantages of the algorithm were proven by experiments.

2. METHODS

Our algorithm consists of three key components. First, the optic nerve is transformed to polar coordinates and modeled as a graph to simplify the computation. This reduces the problem to a graph search for two optimal paths, the rim and the cup. Cost functions are designed for both the rim and the cup, and incorporate information from different features. The cost functions are then used to compute two optimal closed paths through the transformed image of the optic nerve using a graph search algorithm developed by Chen, Wang, Wu [3].

Contact information: michael-merickel@uiowa.edu

2.1. Problem Modeling

The fundamental approach to segmenting the borders of the rim and cup in the optic nerve is to model the rim and the cup as two closed borders. The cup is assumed to be inside of the rim. The optic nerve is *unwrapped* into polar coordinates using the transformation described by Chen, Wang, Wu [3]. The kernel point Q from which the optic nerve is unwrapped is determined as the approximate center of the cup. Q must be within the cup in order for the transformation to be valid. The optic nerve is sampled from Q radially outward with I rays of radius R and J samples per ray. The result of the transformation to polar coordinates is a new 2-D image $P(i, j)$ where $0 \leq i < I$ and $0 \leq j < J$. An example of the transformation can be seen in Figure 3b.

The transformed image P can be viewed as a 2-D weighted, directed graph $G = (V, E)$ (see Figure 1) such that each pixel $P(i, j)$ corresponds to a vertex in V and the edges of E correspond to the connections between pixels to form feasible borders of the rim and the cup.

Since the rim and cup boundaries are smooth, the segmented borders should be sufficiently “smooth”, that is, any two adjacent pixels on the border should not be too far apart. Precisely, a smoothness constraint M exists in which a vertex V at the point (i, j) is said to have a directed edge from itself to every point $(i + 1, j \pm q)$ where $0 \leq q < M$ and $j - q \geq 0$ and $j + q < J$.

The cost of a vertex in V is inversely proportional to the likelihood that it is located on the desired border. In this way we define cost functions for the rim and the cup and the problem is reduced to tracing two optimal paths p_{rim} and p_{cup} in G respectively for the rim and the cup borders, where $0 \leq p_{rim}(i), p_{cup}(i) < J$ for every $0 \leq i < I$. The optimality of a path is defined with respect to the total cost of the vertices on it.

2.2. Cost Function Design

A priori classification is a very significant portion of the information incorporated into the cost functions for both the cup and the rim [4]. In order to utilize the classification information in a smart way we need to associate some cost with the particular regions. For both the rim and the cup, the classified image $\mathcal{C}(x, y)$ is unwrapped using the same parameters and kernel point Q as used when transforming the optic nerve head (see §2.1). The classification is done on a per-pixel basis and thus results in a noisy classification that is inconsistent and lacks smooth and distinct borders. In order to create an approximate border for the rim (resp. cup) we transform the problem into a graph search for an optimal path (border). This is done by defining a cost function for the classification that is inversely proportional to the edge strength of the rim (resp. cup), where the edges are found using a simple edge detector [5]. We utilize an efficient graph searching algorithm [3] to determine the optimal closed path representing the approximate edge of the rim (resp. cup) using an appropriate smoothness constraint ($M = 2$). The determined path is then smoothed with a Gaussian smoothing operation ($\sigma_{rim} = 15.0$ and $\sigma_{cup} = 9.0$) to create an approximate region b_{rim} (resp. b_{cup}) where the rim (resp. cup) might lie. These regions are used as features in the segmentation of both the rim and the cup.

The rim is more consistent and well-defined than the cup, thus by finding it first we are able to constrain the space in which the cup may be located. The three features used in the cost function are edge strength $e(i, j)$, texture $t(i, j)$ and the a priori approximated border $b_{rim}(i, j)$. A cost function $c_{rim}(i, j)$ is defined for the rim based on a weighted combination of features.

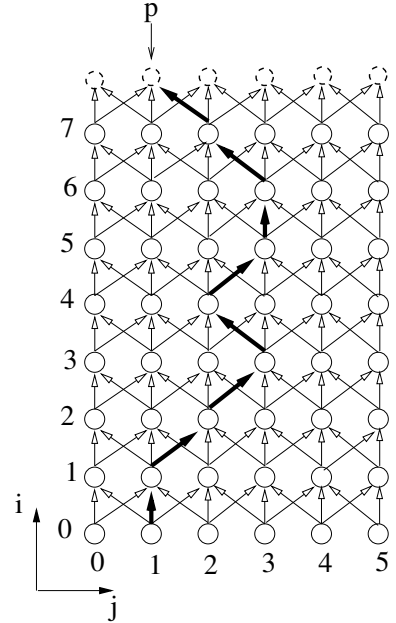


Figure 1. A 2-smoothness graph constructed from the unwrapped image. Path p represents a possible a closed path through the graph.

$$c_{rim}(i, j) = A \cdot b_{rim}(i, j) + B \cdot t(i, j) + C \cdot e(i, j) \quad (1)$$

The edge strength e is determined using a difference of Gaussians (DoG) [5]. Accounting for noise, we set $\sigma_1 = 3.0$ and approximate a Laplacian of Gaussians using the relationship $\sigma_2 = 1.6\sigma_1$ [6]. The DoG is computed only along J , across each sampled ray, thus the edge strength is weighted radially on the optic nerve.

Texture information t is computed for the optic nerve on a per-pixel basis such that

$$t(i, j) = AVG_{right}(i, j) - AVG_{left}(i, j)$$

where $AVG_{right}(i, j)$ (resp. $AVG_{left}(i, j)$) is defined as the average intensity of a floating window on the right (resp. left) of the pixel (i, j) . This can be viewed as the difference between the smoothness on the right of (i, j) and the smoothness on the left of the (i, j) . It is a simplified version of the analysis used in [7] where the gradient of the rim is assumed to lie along j .

Features t , e and b are normalized linearly between 0 and 1 in order to combine the features in a meaningful way. The weighting factors A , B , C utilized in Eq. (1) are determined experimentally using a supervised optimization process in which different solutions to the problem $A + B + C = 1$ are tested. The combination producing the best border positioning errors (see §3.3) was determined to be $A = B = C = \frac{1}{3}$.

Cup segmentation is reduced to determining a smooth path through the a priori classification. However, a structural requirement of the rim/cup relationship is that the cup must lie within the rim. Thus, using the rim segmentation p_{rim} , we can influence the cost function such that the newly determined path must lie inside p_{rim} . In this way the cost function for the cup can be expressed as

$$c_{cup}(i, j) = \begin{cases} \max b_{cup} - b_{cup}(i, j) & \text{if } p_{rim}(i) < j \\ \infty & \text{else} \end{cases} \quad (2)$$

such that the cost is constrained and inversely related to the classification.

2.3. Optimal Path Computation

The rim and the cup are closed borders, thus in polar coordinates $p_{rim}(0) = p_{rim}(I)$. The Chen, Wang, Wu [3] algorithm facilitates this fact with a new and efficient graph search algorithm. The graph search takes advantage of the fact that two optimal paths starting at two different points, $(0, j')$ and $(0, j'')$ ($j' \neq j''$), can be found that do not cross each other. Following from this property is a *divide-and-conquer* algorithm in which the optimal path p_0 beginning at the point $(0, \lfloor \frac{J}{2} \rfloor)$ is computed. The graph is then divided into two subgraphs G_1 and G_2 along p_0 and the algorithm is recursively called on G_1 and G_2 to find the optimal closed paths p_1 and p_2 in G_1 and G_2 , respectively. The optimal closed path in G is the path with a minimum cost among p_0 , p_1 and p_2 . This divide-and-conquer paradigm yields an improvement of nearly an order of magnitude over previous algorithms [8]. The smoothness constraint is set at $M = 2$ to produce smooth borders. A dynamic programming algorithm is used to compute the optimal path beginning at a specific point $(0, j)$. The optimal closed path is then back-traced from the point (I, j) thus beginning and ending at the same point. In this way, we obtain the optimal paths p_{rim} and p_{cup} for the rim and the cup, respectively.

Once the borders of the rim and cup, p_{rim} and p_{cup} respectively, have been determined they can be combined into the polar image $P(i, j)$. $P(i, j)$ can then be transformed using the inverse of the polar transform discussed above to obtain the segmented image $S(x, y)$, which is the output of our algorithm.

3. EXPERIMENTAL METHODS

3.1. Data

Stereo photographs were obtained from 101 patients with a diagnosis of glaucoma. Color slide stereo photographs centered on the optic nerve head were acquired using a fixed geometry Nidek 3Dx stereo retinal camera. This camera takes simultaneous left and right stereo photographs of the optic disc on slide film; after development,

the slides were scanned at 4096×4096 pixel resolution, 24 bit color depth, with a Kodak slide scanner (Kodak Inc., Rochester, NY). See Figure 2.

The Nidek 3Dx camera projects two alignment marks onto the retina that are photographed simultaneously with the optic nerve head. Mutual information based affine registration was used to align the right and left stereo pairs. The image was then cropped to 512×512 pixels keeping the optic nerve head in the center.

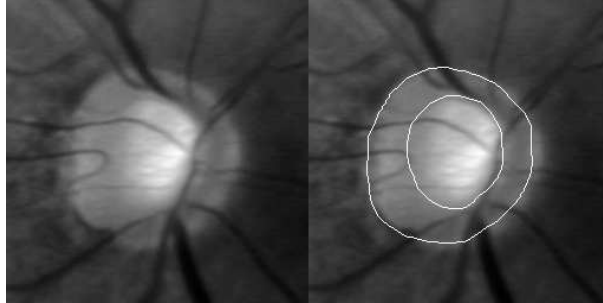


Figure 2. The left image contains the right image from a stereo pair and on the right is the same image overlaid with the reference standard. The innermost region is the cup, and the outermost border is the boundary of the rim.

3.2. Independent Standard

Three ophthalmologists, widely respected glaucoma specialists, carefully marked all pixels of cup and rim on each of the left images of the stereo pair. Planimetry of the stereo pairs using a stereo viewer was utilized. The experts were requested to include blood vessels into their classification of the surrounding tissue; in other words a part of a vessel surrounded by a cup was classified as cup. Three-class reference standards were obtained by a hard winner-take-all threshold of the three expert classifications. The three classes are rim, cup and background.

3.3. Error Indices and Data Analysis

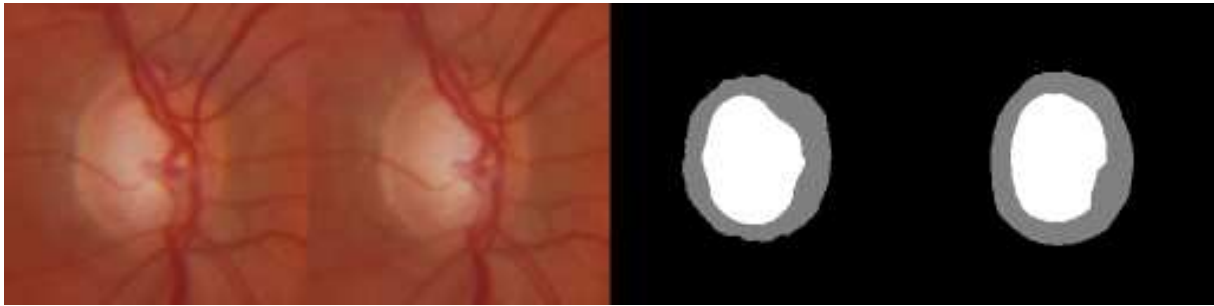
To objectively compare computer-detected borders against the reference standards, maximum border positioning errors, signed mean border positioning errors and root-mean-square border positioning errors will be computed and expressed in pixels and in micrometers where one pixel is approximately $8 \times 8 \mu m^2$. Corresponding points will be defined as pairs of points, the first point being from a computer detected border and the second point from the reference standard border that is closest to each other using the Euclidean distance metric. The positioning errors will be defined as the minimum distance from each computer-detected border pixel to reference standard.

4. RESULTS

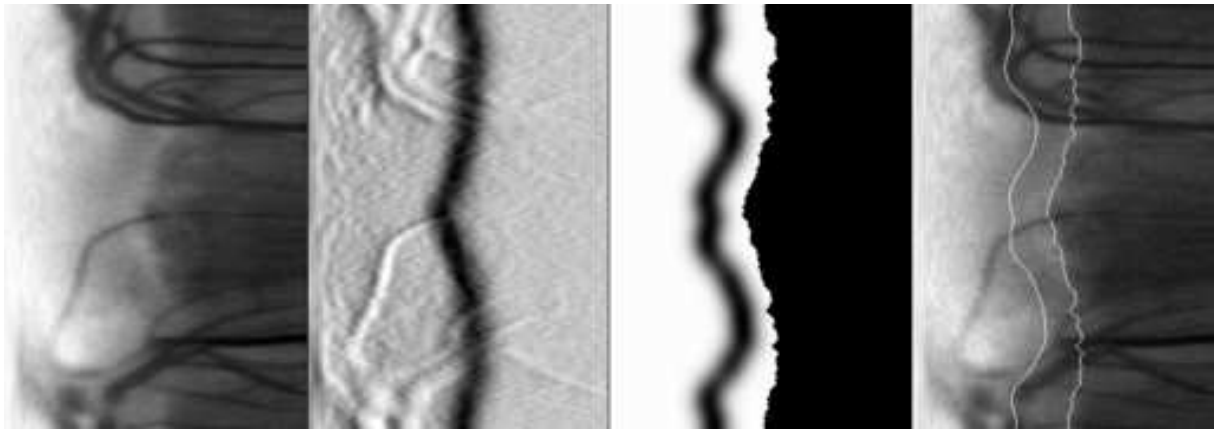
Our algorithm has been implemented and validated using the 101 datasets and a reference standard (see §3). Average border positioning errors are displayed in Table 1. The average signed distance reflects a tendency to underestimate the size of the cup and overestimate the size of the rim. Examples of the cost functions for the rim and the cup can be seen in Figure 3. The output of the algorithm can be seen in Figure 4. Through visual inspection there is one complete failure in the 101 datasets.

5. DISCUSSION

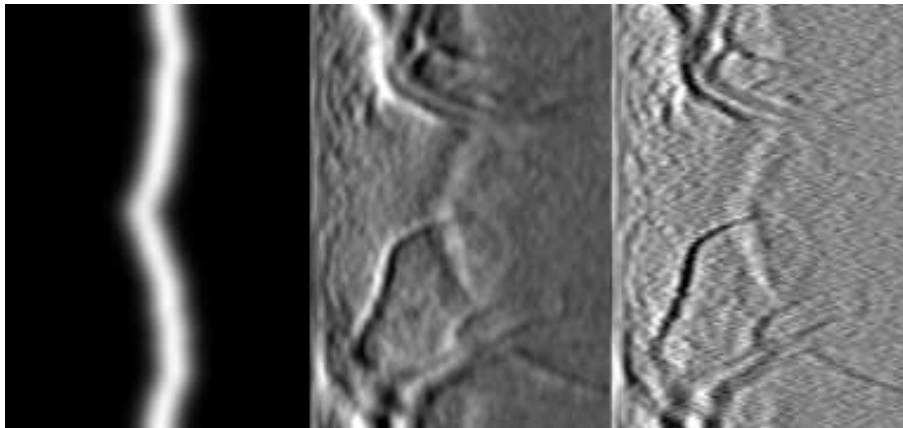
The benefits of our algorithm can be seen in the flexibility to incorporate different features into the cost functions and segment the image into two distinct and smooth regions. This is a big advantage over pixel classification approaches that often cannot guarantee that structural requirements are met. Pixel classification has the advantage of inherent learning approaches such as supervised training [9]. A hybrid approach makes sense in which our algorithm treats the segmentation as a post-processor to the pixel classification. As a result, our algorithm



(a)



(b)



(c)

Figure 3. Intermediate examples of the segmentation algorithm. From left to right, (a) contains the original stereo retinal image, the output of our algorithm, and the reference standard. (b) shows (from left to right) the optic nerve transformed to polar coordinates ($I = 360$, $J = 256$), along with the rim cost function and the cup cost function and the resulting segmentation where the cup is the leftmost border. (c) shows the intermediate features used in the rim segmentation. From left to right, they are the classification region, texture information and the edge strength.

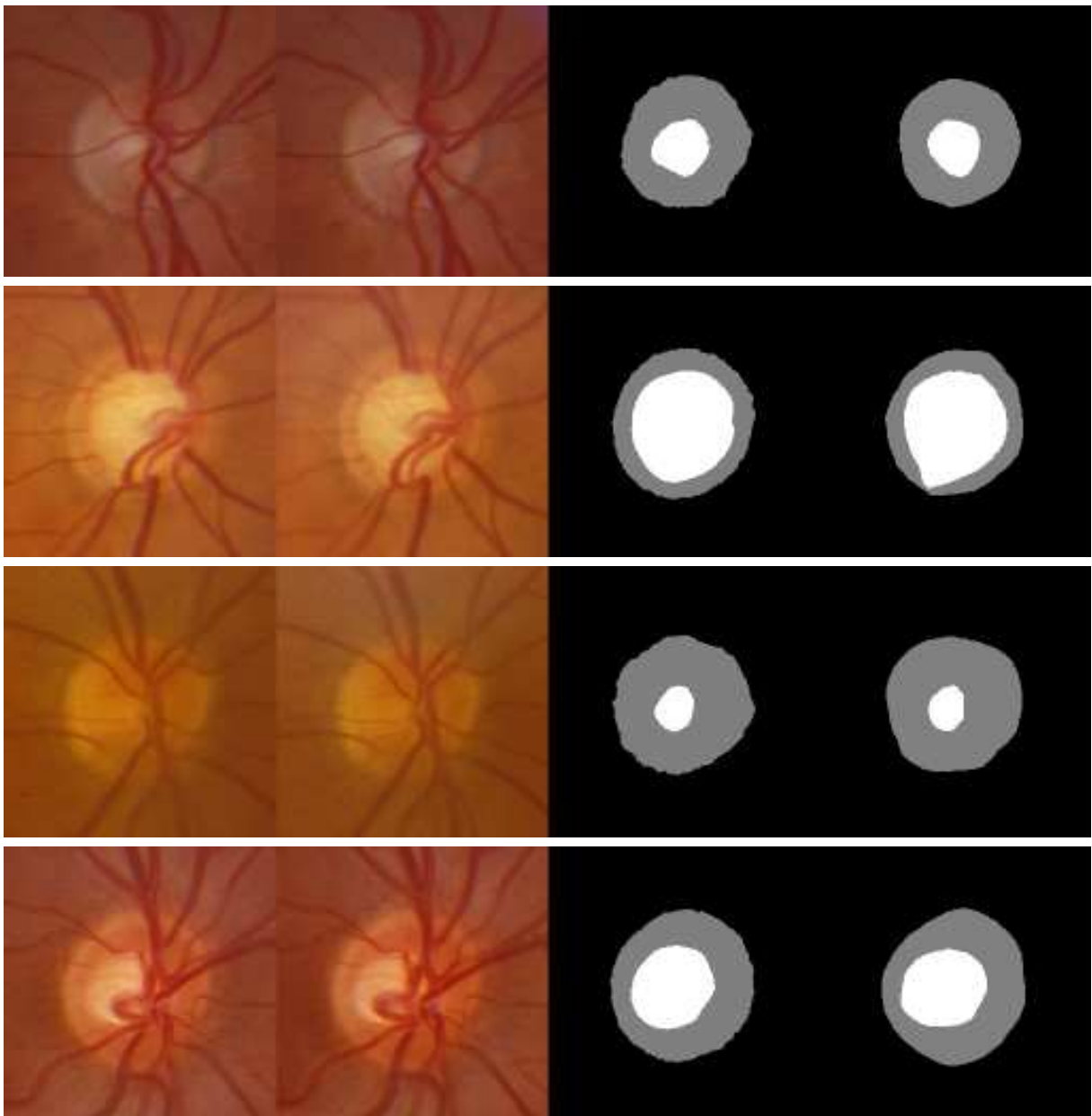


Figure 4. Computer-based segmentation of the optic nerve head. From left to right, left and right stereo color images, computer segmentation, and reference standard by three glaucoma specialists. Black background, gray rim, and white cup.

Table 1. Border Positioning Errors

Metric	Cup		Rim	
	pixels	μm	pixels	μm
Signed Distance	-0.26 ± 6.60	-2.08 ± 52.81	0.03 ± 5.42	0.21 ± 43.37
RMS Distance	6.47 ± 4.98	51.79 ± 39.87	6.18 ± 3.95	49.44 ± 31.58
Max Distance	13.39 ± 7.52	107.14 ± 60.16	13.62 ± 6.89	108.94 ± 55.14

is highly dependent on the quality of the a priori classification. This dependency can be lessened by the incorporation of other features into the cost function, however the largest difficulty in the segmentation is dealing with the quality of the images.

In the stereo color images of the optic nerve there is very poor contrast between the background, the rim and the cup. This problem can be seen clearly in Figure 2. To reduce the effects of poor contrast in the segmentation there are some potential methods to investigate. Currently the segmentation is based on the right image in the stereo pair. Incorporation of the stereo information present in the images could result in a better signal to noise ratio and improved contrast. Also, the current texture information is simple and can be improved using new minimum-variance cost functions proposed by Chan and Vese [10] which are more sensitive to small changes in texture. The benefits of such texture information can be readily seen in [11].

A feature that has not been investigated is the elliptic structure inherent in both the rim and the cup. This information could be useful in the segmentation because in polar coordinates the behavior of an elliptic structure is predictable and could possibly be used to improve the accuracy of the segmentation.

A benefit of our algorithm is that it is feasible for use in a clinical setting. The algorithm is efficient and the results can be validated quickly through visual inspection. The goal is to determine the extent of the rim and the cup for use in determining the cup-to-disc ratio, however a result with only numbers is nonintuitive and does not facilitate adoption in the community.

6. CONCLUSION

An algorithm has been developed and validated against clinical data capable of segmenting the rim and cup of the optic nerve head in stereo retinal images. The transformation of the problem into a graph search for two optimal paths in polar coordinates and the incorporation of smoothness constraints provides a flexible means for modeling the segmentation of the rim and the cup. Results can be quickly validated through visual inspection of the segmentation which is important when used in a clinical setting.

REFERENCES

1. A. Heijl, M. C. Leske, B. Bengtsson, L. Hyman, and M. Hussein, "Reduction of intraocular pressure and glaucoma progression: results from the early manifest glaucoma trial," *Archives of Ophthalmology* **120**, pp. 1268–1279, Oct. 2002.
2. J. M. Tielsch, J. Katz, H. A. Quigley, N. R. Miller, and A. Sommer, "Intraobserver and interobserver agreement in measurement of optic disc characteristics," *Ophthalmology* **95**, pp. 350–356, Mar. 1998.
3. D. Z. Chen, J. Wang, and X. Wu, "Image segmentation with asteroidity/tubularity and smoothness constraints," *International Journal of Computational Geometry and Applications* **12**, pp. 413–428, Oct. 2002.
4. M. D. Abramoff, M. Sonka, W. L. Alward, and Y. H. Kwon submitted to *Investigative Ophthalmology and Visual Sciences*, 2005.
5. M. Sonka, V. Hlavac, and R. Boyle, *Image Processing, Analysis, and Machine Vision*, Brooks/Cole Publishing Company, second ed., 1999.
6. D. Marr and E. C. Hildreth, "Theory of edge detection," *Royal Society of London Proceedings Series B* **207**, pp. 197–217, Feb. 1980.

7. M. Brejl and M. Sonka, "Object localization and border detection criteria design in edge-based image segmentation: Automated learning from examples," *IEEE Transactions on Medical Imaging* **19**, pp. 973–985, Oct. 2000.
8. D. R. Thedens, D. J. Skorton, and S. R. Fleagle, "Methods of graph searching for border detection in image sequences with applications to cardiac magnetic resonance imaging," *IEEE Transactions on Medical Imaging* **14**(1), pp. 42–55, 1995.
9. R. O. Duda, P. E. Hart, and D. G. Stork, *Pattern Classification*, Wiley-Interscience, second ed., 2001.
10. T. F. Chan and L. A. Vese, "Active contours without edges," *IEEE Transactions on Image Processing* **10**, pp. 266–277, Feb. 2001.
11. K. Li, X. Wu, D. Z. Chen, and M. Sonka, "Optimal surface segmentation in volumetric images – a graph-theoretic approach," *IEEE Transactions on Medical Imaging* **28**, pp. 119–134, Jan. 2006.